

Effect of cation disorder on the magnetic properties of $\text{Sr}_2\text{Fe}_{1-x}\text{Ga}_x\text{ReO}_6$ ($0 < x < 0.7$) double perovskites

Alexandra Jung, Irene Bonn, Vadim Ksenofontov, Martin Panthöfer, Sergey Reiman, Claudia Felser, and Wolfgang Tremel
Institut für anorganische und analytische Chemie, Johannes Gutenberg-Universität Mainz, D-55099 Mainz, Germany

(Received 17 November 2006; revised manuscript received 16 February 2007; published 9 May 2007)

The effect of diamagnetic dilution of the Fe sublattice on the structural and magnetic properties of the double perovskite $\text{Sr}_2\text{Fe}_{1-x}\text{Ga}_x\text{ReO}_6$ ($0 < x < 0.7$) has been explored by means of x-ray structural analysis, magnetometry, Mössbauer spectroscopy, and band structure calculations. The end member of the solid solution series, $\text{Sr}_2\text{GaReO}_6$, was predicted to be a half-metallic ferromagnet based on *ab initio* band structure calculations using the WIEN2k software package. Because the Re-containing double perovskites, like the parent compound $\text{Sr}_2\text{FeReO}_6$, rarely exhibit antisite disorder, the appearance of increasing amounts of antisite disorder in $\text{Sr}_2\text{Fe}_{1-x}\text{Ga}_x\text{ReO}_6$ ($0 < x < 0.7$) is unexpected. Although the amount of antisite disorder increases with increasing Ga content, it also depends on the sample preparation history. For $0 < x < 0.4$ only a tetragonal, magnetically ordered phase was detected by x-ray structural analysis as well as Mössbauer analysis. A phase separation into a tetragonal and a cubic phase for $x \geq 0.4$ is detected by x-ray structural analysis accompanied by the observation of a magnetically ordered and a paramagnetic phase in the corresponding Mössbauer spectra. Below 20% Ga content, Ga statistically dilutes the -Fe-O-Re-O-Fe- double-exchange pathways. Phase separation begins at 20% Ga substitution; between 20% and 40% of Ga content, the paramagnetic Ga-based phase does not contain any Fe. The Fe-containing, paramagnetic cubic phases which can be detected by Mössbauer spectroscopy first appear for $x=0.4$.

DOI: 10.1103/PhysRevB.75.184409

PACS number(s): 75.50.Cc, 72.25.Ba, 71.20.-b, 82.80.Ej

I. INTRODUCTION

Double perovskites of the general formula $A_2MM'O_6$, (A =alkaline earth metal, $M=3d$ transition metal), and M' =transition metal, have recently attracted much attention due to the discovery of tunneling magnetoresistance (TMR) at room temperature and at low magnetic fields in powder samples.^{1,2} Therefore, some members of the double-perovskite group can be considered as prospective for spintronic applications.^{3,4} In the ideal cubic modification, double perovskites consist of a rocksalt arrangement of corner-sharing MO_6 and $M'O_6$ octahedra (Fig. 1). The large- A cations are situated in the “cube” voids between the octahedra. Double perovskites exhibit an extreme structural flexibility; e.g., cubic, tetragonal, orthorhombic, and monoclinic structure variants have been reported.⁵⁻¹² In spite of this diversity of structures, the reason for a wide variety of magnetic properties (ferrimagnetism, ferromagnetism, and antiferromagnetism, itinerant and localized magnetism, metals, semiconductors, and insulators) and especially for the half-metallic behavior of the compounds $A_2FeM'O_6$ (A =Sr, Ba; M' =Mo, Re) (Refs. 1, 2, and 13–15) is due to the same mechanism. The Zener double exchange^{16,17} mediates the electron interaction along the axes of the cubic unit cell along the Fe-O- M' units via the oxygen bridges, forming double-exchange pathways -Fe-O- M' -O-Fe-. Thereby, the long-range interaction Fe-Fe and M' - M' is ferromagnetic, whereas the short-range interaction between Fe and M' atoms is antiferromagnetic, leading to ferromagnetic, ferrimagnetic, or antiferromagnetic behavior depending on the electron count of the participating atoms.^{18,19}

Surprisingly, this double-exchange mechanism seems to be retained even if one of the cations M and M' is replaced by a metal with a closed d shell—e.g., Mg or Zn—which is

expected to block the pathways of the electronic interaction.^{17,20,21} Results concerning the double perovskite $A_2\text{Fe}_{1-x}\text{Mg}_x\text{M}'\text{O}_6$ (A =Ca, Sr, Ba; M' =Mo, Re) (Refs. 17 and 20) point to itinerant ferromagnetic behavior for the whole solid solution series $\text{Sr}_2\text{Fe}_{1-x}\text{Ga}_x\text{ReO}_6$ ($0 < x < 0.8$).

Sher *et al.*¹⁷ as well as Bramnik *et al.*²⁰ report on the magnetic properties of $A_2\text{Fe}_{1-x}\text{Mg}_x\text{M}'\text{O}_6$ which reveal that the long-range ferromagnetism of the compounds is conserved up to the highest Mg substitution levels. In contrast, Kato *et al.* report $\text{Sr}_2\text{ZnReO}_6$ to be antiferromagnetic below $T_N=20$ K with long-range ferromagnetic clusters due to spin frustration.²¹

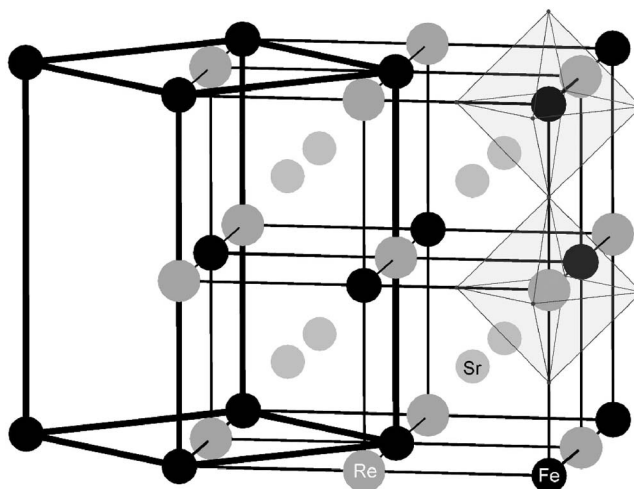


FIG. 1. Crystal structure of the double perovskite $\text{Sr}_2\text{FeReO}_6$: Fe (black), Re (dark gray), Sr (light gray), and O (octahedra); the cubic unit cell is drawn in thin black lines, the tetragonal unit cell in thick black lines.

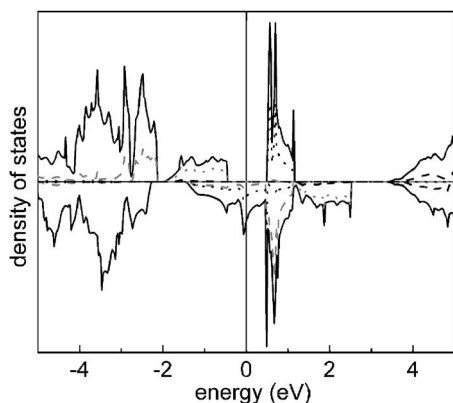


FIG. 2. Density of states of $\text{Sr}_2\text{FeReO}_6$ in the ideal cubic structure as proposed by Kobayashi *et al.* (Ref. 2), total DOS (solid black), partial DOS of Re dt_{2g} (black spotted), partials DOS of Re de_g (black dashed), partial DOS of Fe de_g (gray spotted), and partial DOS of Fe dt_{2g} (gray dashed).²²

Generally, the magnetic properties of double perovskites can be estimated by means of band structure calculations within the van Hove framework.^{1,2,22–26} In most cases the calculated and experimental properties match rather well. For $\text{Sr}_2\text{FeMoO}_6$, $\text{Sr}_2\text{FeReO}_6$,^{1,2,27} $\text{Ba}_2\text{FeReO}_6$,^{27,28} and $\text{Sr}_2\text{CrReO}_6$,^{29,30} the observed metallic and magnetic properties agree well with the results of band structure calculations, predicting half-metallic ferrimagnetic compounds in all four cases. These half-metallic properties require a large density of states at the Fermi level [$\text{DOS}(E_F)$] for one spin direction, whereas the other spin direction must be insulating (Fig. 2). In the insulating spin direction five electrons reside in the $3d$ states of Fe, whereas the $5d$ ($4d$) states of Re (Mo) are empty. As the stoichiometry of $\text{A}_2\text{FeM}'\text{O}_6$ dictates that the combined oxidation states of Fe and Re (Mo) sum up to +8, the remaining two (one) electrons are located in the conduction band of the metallic spin direction which is composed of the t_{2g} states of Fe and Re (Mo). Another example of the predictability of magnetic and electronic properties by means of band structure calculations is the observed transition of the ferrimagnetic metal $\text{Sr}_2\text{FeReO}_6$ to the antiferromagnetic insulator $\text{Sr}_2\text{FeSbO}_6$ along the series of solid solutions $\text{Sr}_2\text{FeRe}_{1-x}\text{Sb}_x\text{O}_6$.²³ Using the WIEN2k software package³¹ $\text{Sr}_2\text{FeSbO}_6$ was found to be a spin-polarized insulator without any Sb states participating in the DOS at the Fermi level which was experimentally confirmed subsequently by conductivity and Mössbauer spectroscopy investigations.²³

The results of band structure calculations have been used successfully to vary and optimize the magnetization, Curie temperature, and TMR effect of double perovskites systematically by “doping”—i.e. adjusting the electron count of the target compounds to their optimum values. For the series of solid solutions $\text{Sr}_2\text{Fe}_{1-x}\text{Cr}_x\text{ReO}_6$ the essential features of materials exhibiting a large TMR effect could be improved.²² The saddle point (the so-called van Hove instability) is adjusted at the Fermi level for Cr doping levels of approximately 25%, and the Curie temperatures could be increased along the series of solid solutions.

In this contribution we study the influence of the main group metal Ga on the Fe(M) site of the double perovskite

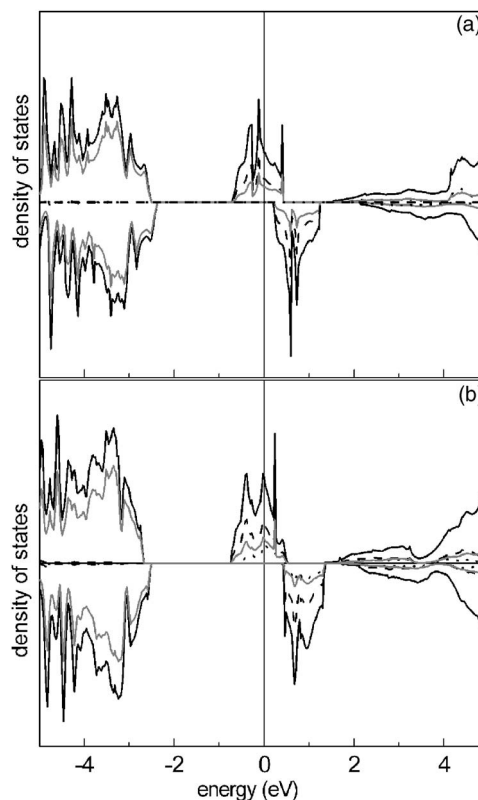


FIG. 3. Density of states of $\text{Sr}_2\text{GaReO}_6$ (a) calculated in space group $Fm-3m$, total DOS (solid black), partial DOS of Re de_g states (black spotted), partial DOS of Re dt_{2g} states (black dashed), and partial DOS of O (solid gray) and (b) calculated in space group $I4/m$, total DOS (solid black), partial DOS of Re de_g (black spotted), partial DOS of Re dt_{2g} (black dashed), and partial DOS of O (solid gray).

$\text{A}_2\text{FeM}'\text{O}_6$ on the double-exchange mechanism. Surprisingly, the results of spin-polarized *ab initio* band structure calculations for $\text{Sr}_2\text{GaReO}_6$ using the WIEN2k software package³¹ illustrated as the DOS in Fig. 3 reveal that the diamagnetic dilution of the Fe sublattice with the main group metal Ga preserves the half-metallic nature of $\text{Sr}_2\text{FeReO}_6$. Here we report the synthesis of single-phase material of the solid solution series $\text{Sr}_2\text{Fe}_{1-x}\text{Ga}_x\text{ReO}_6$ up to Ga content of $x=0.7$ together with the related band structure, crystal structures, and magnetic properties.

II. EXPERIMENT

Starting materials were reagent-grade SrO (Aldrich, 99.9%), Fe_2O_3 (Alfa Aesar, 99.99%), Ga_2O_3 (Aldrich, 99.99%), Re metal, and Re_2O_7 (Alfa Aesar, 99.9%). All starting materials are stored under argon (Braun Labmaster) and examined by x-ray powder diffraction before use.

The $\text{Sr}_2\text{Fe}_{1-x}\text{Ga}_x\text{ReO}_6$ samples were prepared by high-temperature solid-state reactions. Because of the strongly hygroscopic properties of SrO and the large vapor pressure of Re_2O_7 , the samples were prepared in an inert gas atmosphere in a glove box. Stoichiometric amounts of SrO, Fe_2O_3 , Ga_2O_3 , Re, and Re_2O_7 [$2\text{SrO}:(1-x)/2 \text{Fe}_2\text{O}_3:x/2$

$\text{Ga}_2\text{O}_3:0.3 \text{ Re}:0.35 \text{ Re}_2\text{O}_7]$ were ground in an agate mortar and pressed into pellets. In order to avoid Sr attack on the quartz tubes these pellets were transferred into corundum containers and finally sealed in evacuated quartz tubes. The samples were annealed for 7 days at 1000 °C. Thereafter they were rapidly cooled to room temperature by quenching in an ice water mixture. The heat capacity of the corundum containers prevents a very fast and homogeneous cooling of the macroscopic sample. This fact explains the observed nonhomogeneity of the samples discussed below.

X-ray powder diffraction measurements were performed using a Siemens D5000 with monochromatized Cu $K\alpha$ radiation [Ge (220) monochromator]. Lattice constants (relative to Si, which was used as internal standard) were obtained by Rietveld refinement applying the fundamental parameter approach (TOPAS Academic³²).

The variable-temperature magnetic susceptibility measurements of $\text{Sr}_2\text{Fe}_{1-x}\text{Ga}_x\text{ReO}_6$ were performed using a Quantum Design MPMS-XL superconducting quantum interference device (SQUID) magnetometer, equipped with a high-temperature furnace. Experimental data were corrected for diamagnetism using Pascal's constants.³³

Mössbauer measurements of $\text{Sr}_2\text{Fe}_{1-x}\text{Ga}_x\text{ReO}_6$ powder samples were done in transmission geometry using a constant-acceleration spectrometer and a helium bath cryostat. ^{57}Fe Mössbauer spectra were recorded between room temperature and 4.2 K using a 50 mCi $^{57}\text{Co}(\text{Rh})$ source. The RECOIL 1.03 Mössbauer Analysis Software was used to fit the experimental spectra.³⁴ Isomer shift values are quoted relative α -Fe at 293 K.

Band structure calculations were performed within the full-potential augmented plane-wave (FLAPW) framework within the generalized gradient approximation (GGA) using the WIEN2k software package.³¹ The crystal structure of $\text{Sr}_2\text{GaReO}_6$ was estimated in two different ways. One calculation used the reported cubic structure with lattice parameter $c=7.84 \text{ \AA}$.^{35,36} Since no further structural details are given in Refs. 35 and 36, the electronic structure of $\text{Sr}_2\text{GaReO}_6$ was calculated using the structure model of Kobayashi *et al.*² The second calculation was performed for $\text{Sr}_2\text{GaReO}_6$ in a tetragonal setting (space group $I4/m$, $a=5.54 \text{ \AA}$, $c=7.84 \text{ \AA}$) approximated from the crystal structure parameters of $\text{Sr}_2\text{Fe}_{0.3}\text{Ga}_{0.7}\text{ReO}_6$ and $\text{Sr}_2\text{Fe}_{0.4}\text{Ga}_{0.6}\text{ReO}_6$ (*vide infra*). The number of k points in the irreducible Brillouin zone was 20. The convergence criterion was fixed to 0.0001 Ry.

III. RESULTS

A. Electronic structure

The electronic structure of the hitherto unknown end member of the series of solid solutions $\text{Sr}_2\text{Fe}_{1-x}\text{Ga}_x\text{ReO}_6$, $\text{Sr}_2\text{GaReO}_6$, was calculated using the WIEN2k software package.³¹ The calculation was performed for the two different possible models of the crystal structure: (i) the ideal cubic configuration as suggested by Kobayashi *et al.*¹ and (ii) the tetragonal configuration in space group $I4/m$ estimated based on the observed structure of the samples with $0.1 \leq x \leq 0.7$. In the following discussion the d orbitals of the transition metals will be labeled according to the Cartesian co-

ordinates of the cubic unit cell for both configurations of the double perovskite, the cubic and the tetragonal one. The DOS of $\text{Sr}_2\text{GaReO}_6$ in the cubic and tetragonal configurations [Figs. 3(a) and 3(b)] shows that the diamagnetic dilution of the Fe sublattice by the main group metal Ga preserves the half-metallic ferromagnetic nature of $\text{Sr}_2\text{FeReO}_6$. The DOS is metallic in the spin-up direction comprising states from -1.0 to 0.5 eV , whereas the insulating spin-down direction reveals a band gap of approximately 3.0 eV around E_F . As expected from the lack of d orbitals and in accordance with the fixed $3+$ valence state, Ga does not participate in the DOS near E_F . Surprisingly, $\text{Sr}_2\text{GaReO}_6$ is calculated to be a half-metallic ferromagnet with highly spin polarized Re d -O states in both cubic and tetragonal symmetries. In the ideal cubic case, the Re-O antibonding de_g bands that are responsible for the direct σ^* -type interaction along $[100]$ (axis of the cubic unit cell) are located $\approx 2 \text{ eV}$ above E_F . The Re dt_{2g} orbitals in the vicinity of E_F permit a π^* -type interaction along $[100]$. In spite of the symmetry reduction, the DOS of the tetragonal structure exhibits the same characteristics as that for the cubic case, the main difference being now a small contribution of Re de_g states in the vicinity of E_F in addition to the Re dt_{2g} states which are expected in this energy range. In conclusion, a substitution of Fe by Ga does not destroy the ferromagnetic exchange within the Re sublattice and therefore the overall half-metallic properties of $\text{Sr}_2\text{GaReO}_6$ are preserved.

The spin-polarized band structure of $\text{Sr}_2\text{GaReO}_6$, calculated using the WIEN2k software package,³¹ is presented for the cubic and tetragonal settings of the crystal structure. The band structures for the face-centered-cubic and body-centered-tetragonal Brillouin zones are shown in Fig. 4 and Fig. 6, respectively. In the cubic crystal structure, the band structures of the two different spin directions reveal a remarkable similarity. Below -3.0 eV and above 1.0 eV , the two band structures are virtually identical. In the region between -3.0 and 1.0 eV one bundle of three bands appears which shows an identical run in both spin directions. However, these bands cross E_F in the spin-up direction whereas they are located directly above E_F in the spin-down direction. Therefore, the material shows metallic properties in the spin-up direction and insulating properties in the spin-down direction. In Fig. 4, the band structures of the cubic structure are decorated with the fatbands derived from the different atomic orbitals of $\text{Sr}_2\text{GaReO}_6$. As expected from the DOS, Ga states appear above 1.0 eV in both spin directions and do not have any relevance for the discussion of the bands in the vicinity of E_F [Figs. 4(c) and 4(g)]. The same holds true for the oxygen p states, which contribute mainly to the states below -3.0 eV [Figs. 4(d) and 4(h)]. Furthermore, Re de_g states involved in a σ^* -type bonding along $[100]$ do not contribute to the bands near E_F but share states of higher energy—above 1.0 eV —together with the Ga p states [Figs. 4(b) and 4(f)]. Therefore the band structure close to the Fermi level is dictated by Re-Re interactions. The Re dt_{2g} orbitals are involved in π -type interactions along $[100]$ (axis of the cubic unit cell) and in σ -type interactions along $[110]$ (the face diagonal of the respective unit cell faces). The Re-Re separation along $[100]$ is approximately 7.8 \AA which is compatible with a very weak interaction; the Re-Re sepa-

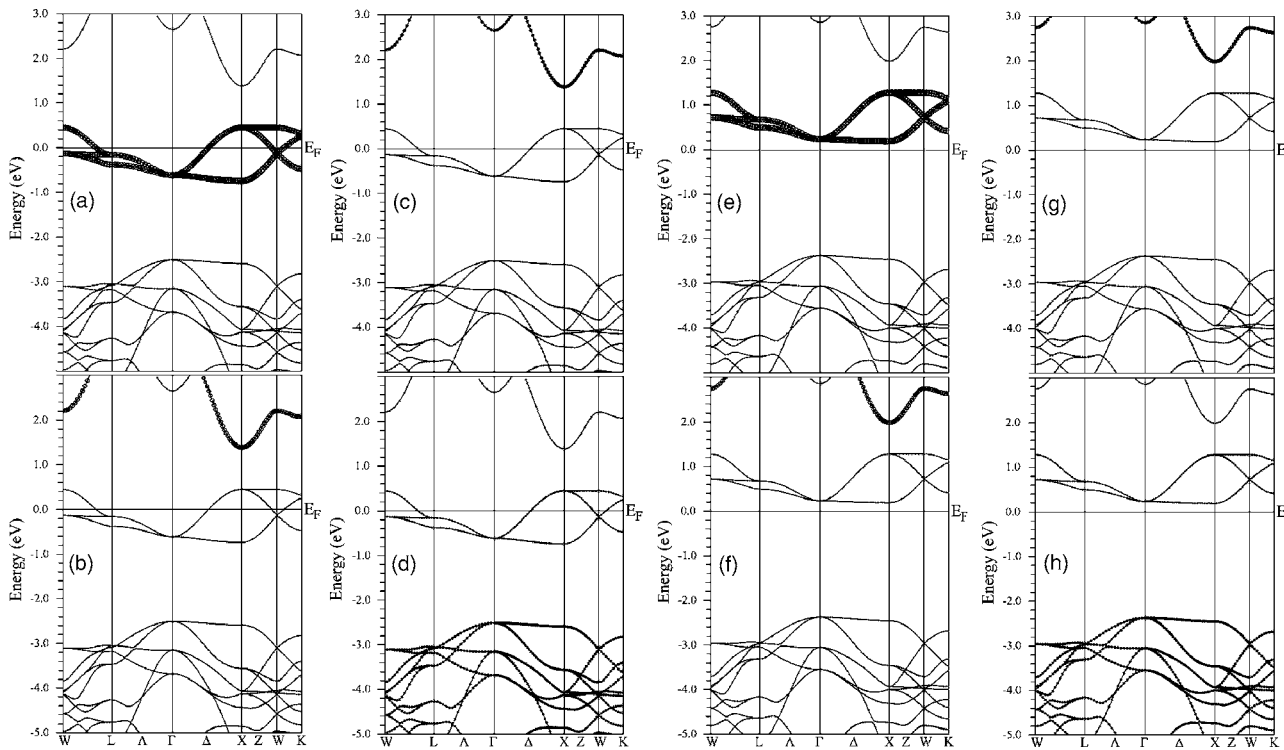


FIG. 4. Band structure of $\text{Sr}_2\text{GaReO}_6$ calculated in space group $Fm\bar{3}m$ decorated with fatbands of the (a) Re d_{xy} , d_{yz} , and d_{xz} states (dt_{2g} , spin up), (b) Re $d_{x^2-y^2}$ and d_{z^2} states (de_g , spin up), (c) Ga states (spin up), (d) O p states (spin up), (e) Re d_{xy} , d_{yz} , and d_{xz} states (dt_{2g} , spin down), (f) Re $d_{x^2-y^2}$ and d_{z^2} states (de_g , spin down), (g) Ga states (spin down), and (h) O p states (spin down).

ration along the face diagonal is approximately 5.5 \AA , which is significantly shorter, but the resulting σ -interaction is still weak (Fig. 5). As a result of the large metal-metal separations the interactions between the Re t_{2g} orbitals are weak, the differences in energy between bonding, nonbonding, and antibonding interaction of the orbitals are small, and the bands are flat.

At the Γ point the Re t_{2g} orbitals contributing to the highlighted band at -0.5 eV (spin up) or 0.5 eV (spin down) are in phase (Fig. 5) and the corresponding Re-Re interactions

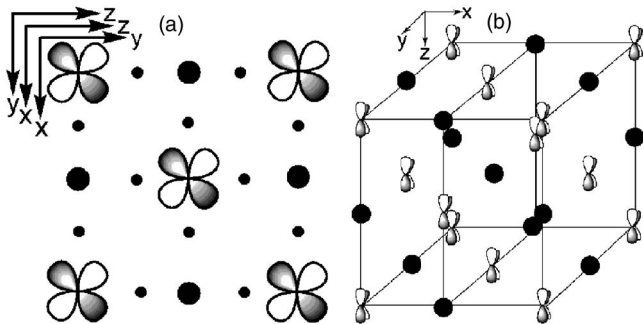


FIG. 5. (a) Interactions of Re d_{xy} , d_{xz} , and d_{yz} orbitals (in white and gray) at -0.5 eV (spin up) and 0.2 eV (spin down) at point Γ of the cubic-face-centered Brillouin zone. The larger black dots replace the Ga atoms, the smaller ones the oxygen atoms whose orbitals do not take part to the interaction of this band. (b) Interaction of Re d_{yz} orbitals (in white and gray) at point Γ of the cubic-face-centered Brillouin zone. The large black dots represent the Ga atoms; the oxygen atoms are omitted.

along $[100]$ are weakly π antibonding. The Re-Re interaction along the face diagonal is of σ -type and therefore stronger, in particular as the Re-Re separation of 5.5 \AA along $[110]$ is significantly shorter than the Re-Re distance along $[100]$. On moving from Γ to X the t_{2g} bands split up into two subbands (a degenerate pair and a nondegenerate partner). Along the x axis the nondegenerate band (d_{yz}) is involved only in δ -type interactions and therefore remains energetically unchanged, whereas the degenerate pair (d_{xy}/d_{xz}) moves up in energy with k . This observation can be rationalized as follows. Along Δ the Bloch factor between the dt_{2g} orbitals changes from 1 to -1 , and therefore the former π -interaction along $[100]$ becomes bonding whereas the former σ -interaction along $[110]$ vanishes. As a result, the degenerate band moves up in energy. Along X - W - K the d_{xy} component of the degenerate pair remains at constant energy, whereas its d_{xz} partner goes down due to an increase in the π -bonding interaction along the face diagonal of the xy plane. In contrast, the vanishing σ -interactions in the face diagonal of the yz plane cause the d_{yz} band to move up.

Along Γ - L , the t_{2g} bands exhibit only a small dispersion. Upon moving from Γ to L a simultaneous phase change occurs in the x , y , and z directions. Due to symmetry restrictions, the Re atoms on $\frac{1}{2}\frac{1}{2}0$ do not contribute to these orbital interactions. The resulting nodes on the face centers lead to a doubling of the relevant Re-Re separations and a concomitant decrease in the σ -type interaction along $[110]$ and of the π^* -interactions along $[100]$. Therefore, the energy of the Re dt_{2g} does not change significantly. The slight splitting of the bands from Γ to L is induced by the different sizes of the

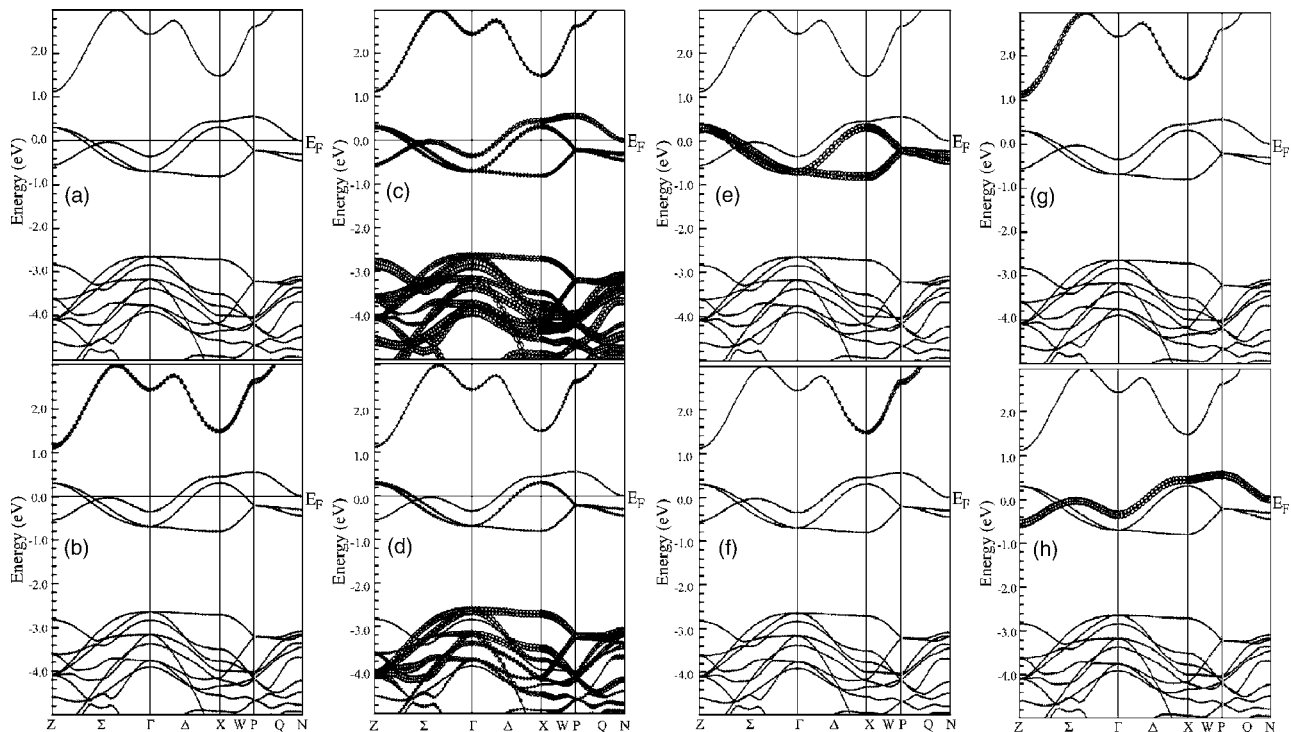


FIG. 6. (a) Band structure of $\text{Sr}_2\text{GaReO}_6$ (tetragonal setting) in the spin-up direction and band structure decorated with “fatbands” of the (b) Ga states, (c) O(1) p states, (d) O(2) p states, (e) Re d_{xz} and d_{yz} states, (f) Re $d_{x^2-y^2}$ states, (g) Re d_{z^2} states, and (h) Re d_{xy} states.

GaO_6 and ReO_6 octahedra and the resulting differences in M -O and M' -O distances.

Figure 6 shows the band structure of $\text{Sr}_2\text{GaReO}_6$ in the tetragonal setting ($I4/m$) in the spin-up direction [Fig. 6(a)] together with the band structures decorated with the fatbands derived from the different atomic orbitals [Figs. 6(b)–6(h)]. The band structure in the spin-down direction is not shown, because it can be derived from the spin-up band structure by shifting the t_{2g} bands situated between -1.0 eV and 0.5 eV in the spin-up direction to energies above the Fermi level. Hence, the band structures calculated in the tetragonal and cubic settings of the double-perovskite structure reveal the same half-metallic band structure. Moreover, the Ga p states [Fig. 6(b)] and the Re e_g states [Figs. 6(f) and 6(g)] appear in the same energy range (above 1.0 eV) as in the cubic setting of the crystal structure. The bands around the Fermi level are composed of the Re t_{2g} states [Figs. 6(e) and 6(h)] and, in contrast to the cubic case, of the O p states [Figs. 6(c) and 6(d)]. Therefore, the Re d orbitals at E_F can interact via the O $2p$ states. Nevertheless, the essential characteristics of the Re d_{xz} and Re d_{yz} orbitals do not differ from those of the cubic case and therefore will not be discussed in detail here. Moreover, the shape of the d_{xy} band in the tetragonal setting does not differ from the band progression of the d_{xy} band in the cubic setting. Due to the participation of the O p states, the orbital interactions are slightly stronger antibonding in the tetragonal case and therefore the Re d_{xy} band is shifted to higher energy by about 0.4 eV.

In summary, the band structure calculation in the idealized cubic crystal structure as well as in the observed tetragonal structure leads to comparable results. $\text{Sr}_2\text{GaReO}_6$ may be expected to be a half-metallic ferromagnet with highly spin-

polarized Re-O states and Ga p states situated well above the Fermi level. Ga is expected to have a fixed valence ($3+$) in this compound. Thus, $\text{Sr}_2\text{GaReO}_6$ is expected to be a magnetic compound composed of nonmagnetic elements. In the sequel, we report the synthesis of single-phase samples of the solid solution series $\text{Sr}_2\text{Fe}_{1-x}\text{Ga}_x\text{ReO}_6$.

B. Structural characterization

The crystal structures of the compounds of the series $\text{Sr}_2\text{Fe}_{1-x}\text{Ga}_x\text{ReO}_6$ ($0 \leq x \leq 0.7$) were determined by x-ray powder diffraction and Rietveld refinements based on the fundamental parameter approach.³² The corresponding x-ray diffraction patterns presented in Fig. 7 reveal that all samples crystallize in ordered double-perovskite structure variants. As an example, the measured x-ray pattern of $\text{Sr}_2\text{Fe}_{0.5}\text{Ga}_{0.5}\text{ReO}_6$ (mixed with Si as internal standard) together with the calculated x-ray patterns of tetragonal $\text{Sr}_2\text{Fe}_{0.5}\text{Ga}_{0.5}\text{ReO}_6$ and cubic $\text{Sr}_2\text{Fe}_{0.5}\text{Ga}_{0.5}\text{ReO}_6$, and the corresponding difference curve are shown in Fig. 8.

For low Ga content the samples are single-phase double perovskites crystallizing in space group $I4/m$ with Sr situated on site $4d$, Fe and Ga on site $2a$, Re on site $2b$, O(1) on site $8h$, and O(2) on site $4e$, revealing no Fe/Re and minor Ga/Re antisite disorder. With increasing Ga content ($x=0.4$), reflection shape asymmetries and reflection splitting afforded the refinement of a second, cubic phase according to the ordered cubic double-perovskite structure [$Pm\bar{3}m$ with Sr situated on site $8g$, Fe and Ga on sites $1a$ and $3c$, Re on sites $1b$ and $3d$, O(1) on site $6e$, O(2) on site $6f$, and O(3) on site $12h$] (Fig. 8). The amount of cubic phase depends upon the sample preparation—i.e., is presumably determined by the

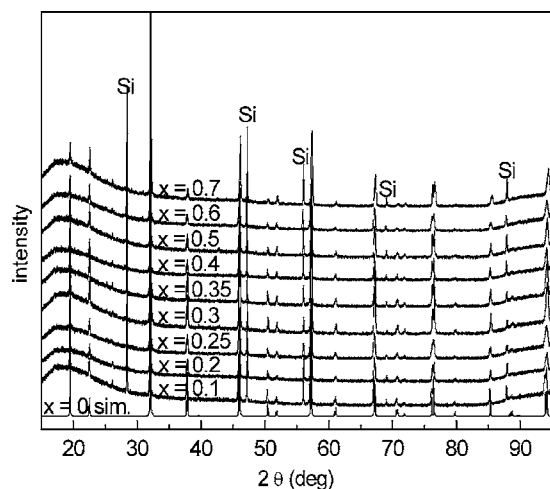


FIG. 7. Calculated x-ray powder diffraction pattern of the ordered double perovskite $\text{Sr}_2\text{FeReO}_6$ in space group $I4/m$ ($x=0$ sim.); measured x-ray diffraction patterns of $\text{Sr}_2\text{Fe}_{1-x}\text{Ga}_x\text{ReO}_6$ for $0.1 \leq x \leq 0.7$ mixed with Si as internal standard.

cooling rate of the sample during the quenching procedure. Nevertheless, it increases monotonously with increasing Ga content (Table I). In the case of the tetragonal phase, no Fe/Re disorder was observed, while the amount of Ga/Re antisite disorder increases up to 17%. In contrast, antisite disorder is present for both transition-metal cation sites in the cubic phase. Again, the amount increases upon increasing Ga content but depends on sample preparation history (Table I). For $\text{Sr}_2\text{Fe}_{0.3}\text{Ga}_{0.7}\text{ReO}_6$ the cubic phase is close to a fully disordered structure. Taking into account the ionic radii of Ga^{3+} , Fe^{3+} , and Re^{5+} [$r(\text{Ga}^{3+})=62$ pm, $r(\text{Fe}^{3+})=65$ pm, $r(\text{Re}^{5+})=58$ pm],³⁷ the observation of an increasing Ga/Re antisite disorder without an Fe/Re disorder can be under-

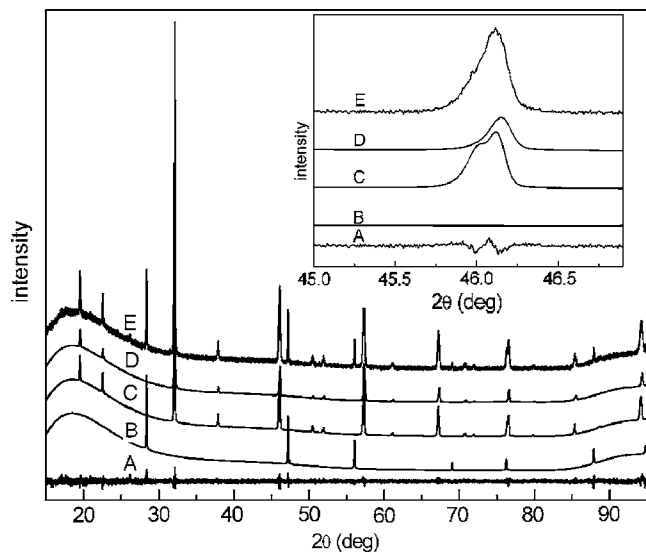


FIG. 8. Measured x-ray powder diffraction pattern of $\text{Sr}_2\text{Fe}_{0.5}\text{Ga}_{0.5}\text{ReO}_6$ mixed with Si as internal standard (E) together with the simulated x-ray patterns of the tetragonal $\text{Sr}_2\text{Fe}_{0.5}\text{Ga}_{0.5}\text{ReO}_6$ (D) and the cubic $\text{Sr}_2\text{Fe}_{0.5}\text{Ga}_{0.5}\text{ReO}_6$ (C), Si (B), and the corresponding difference curve (A).

stood in terms of minimization of structural stress. The observation of a phase segregation into a cubic and a tetragonal double perovskite instead of a pure shift from the tetragonal towards the cubic double-perovskite structure is unexpected, in particular when comparing this series of solid solutions with systems reported earlier.^{22,23}

Lattice parameters a and c of the solid solution series $\text{Sr}_2\text{Fe}_{1-x}\text{Ga}_x\text{ReO}_6$ as obtained by Rietveld refinement are compiled in Table I. As expected from Vegard's rule the dependence of the lattice parameters on the degree of substitution is almost linear, confirming the existence of a continuous solid solution series in the range $0 \leq x \leq 0.7$. The lattice parameters of the cubic and tetragonal phases decrease with increasing Ga content as illustrated in Table I. The decrease of the lattice parameters can be rationalized from the ionic radii of Ga^{3+} and Fe^{3+} .³⁷

The c/a ratio (Table I) is used to gain insight into the dependence of the amount of tetragonal distortion of the tetragonal phase on the Ga doping level. From the relation $c/a = \sqrt{2}$ for a cubic double perovskite one can estimate the degree of tetragonal distortion of the tetragonal phase. The continuous decrease of the c/a ratio indicates a slow decrease of the tetragonal distortion of the tetragonal phase with increasing Ga content. Thus, with increasing Ga content two different effects superimpose: (i) samples containing more than 40% Ga show a phase segregation into a cubic and a tetragonal phase and (ii) the amount of tetragonal distortion of the tetragonal phase decreases with increasing Ga content.

The above results qualitatively agree with the structural behavior expected from an analysis of the tolerance factor t for perovskites of the general formula AMX_3 in Table I. The tolerance factor

$$t = \frac{r(A) + r(X)}{\sqrt{2}[r(M) + r(X)]}$$

describes the interrelation between the perovskite structure and the associated ionic radii taken from Refs. 35 and 37–39. To plot the concentrational dependence of the tolerance factor, one should know the valence state of the ions in the crystal structure. The valence state of iron is of special importance because the ionic radii of Fe^{2+} and Fe^{3+} differ significantly, whereas the ionic radius of Re is practically valence independent. The t values in Table I are based on an iron valence state $\text{Fe}^{2.7+}$ which results from a detailed study of the iron valence states by means of Mössbauer spectroscopy (*vide infra*). The continuous increase of the tolerance factor t with increasing Ga substitution up to a value $t = 0.9095$ for $\text{Sr}_2\text{Fe}_{0.3}\text{Ga}_{0.7}\text{ReO}_6$ supports the experimental results of the c/a ratios (Table I) because perovskites are supposed to crystallize in a cubic unit cell for $t=1$. An increasing tetragonal distortion is expected for $1 > t > 0.8$; i.e., experimental results and the description based on a space filling model are in good agreement.

C. Magnetic measurements

The field dependence of the magnetization at 5 K was measured in order to determine the saturation magnetization of the samples. Based on the hysteresis loops with small

TABLE I. Ga content (x), amount of cubic and tetragonal phase (am_{cub} and am_{tet}), lattice parameters of the cubic and tetragonal phases (c_{cub} , a_{tet} , c_{tet}), $(c/a)/\sqrt{2}$ ratio, tolerance factor t , Re/Fe and Re/Ga disorder ratios (SRF and SRG), and agreement parameters (R_{wp}) of the compounds $\text{Sr}_2\text{Fe}_{1-x}\text{Ga}_x\text{ReO}_6$ ($0 < x < 0.7$).

x	am_{cub} (%)	am_{tet} (%)	c_{cub} (Å)	a_{tet} (Å)	c_{tet} (Å)	$(c/a)/\sqrt{2}$	t	SRF (%)	SRG (%)	R_{wp}
0.1	0	100		5.5600(5)	7.8966(8)	1.0043	0.9002	0	3.87	4.419
0.2	0	100		5.5577(5)	7.8951(8)	1.0045	0.9017	0	3.66	3.512
0.2	0	100		5.5584(5)	7.8912(8)	1.0039	0.9017	0	5.41	4.583
0.25	0	100		5.5579(7)	7.8911(13)	1.0040	0.9025	0	6.45	4.887
0.25	0	100		5.5591(7)	7.8939(10)	1.0041	0.9025	0	6.28	4.765
0.3	0	100		5.5545(8)	7.8840(13)	1.0037	0.9033	0	6.46	3.982
0.3	0	100		5.5573(5)	7.8879(9)	1.0037	0.9033	0	10.35	4.568
0.3	0	100		5.5585(6)	7.8898(10)	1.0037	0.9033	0	10.93	4.987
0.35	0	100		5.5546(6)	7.8850(9)	1.0038	0.9041	0	6.88	4.483
0.4	0	100		5.5532(5)	7.8805(9)	1.0035	0.9048	0	7.95	4.517
0.4		97.63		5.5576(7)	7.886(1)	1.0034	0.9048	0	11.02	4.986
0.4	2.37		7.859(4)				0.9048	0	22.62	4.986
							0.9048	0	0.05	
0.5		89.39		5.5521(9)	7.872(2)	1.0026	0.9064	0	15.62	4.500
0.5	10.61		7.846(2)				0.9064	50.00	15.29	4.500
							0.9064	44.90	50	
0.5		93.99		5.5540(6)	7.878(1)	1.0030	0.9064	0	12.35	4.565
0.5	6.01		7.850(2)				0.9064	35.88	28.65	4.565
							0.9064	50.00	40.59	
0.6		82.54		5.555(1)	7.873(3)	1.0022	0.9079	0	14.49	4.912
0.6	17.46		7.847(2)				0.9079	40.00	15.95	4.912
							0.9079	40.00	46.29	
0.7		80.92		5.552(1)	7.867(2)	1.0020	0.9095	0	16.97	4.509
0.7	19.08		7.845(2)				0.9095	30.00	36.82	4.509
							0.9095	30.00	48.75	

coercive fields (Fig. 9) materials of all compositions can be classified as soft magnetic.

The experimental saturation magnetization of the solid solution series $\text{Sr}_2\text{Fe}_{1-x}\text{Ga}_x\text{ReO}_6$ ($0 < x < 0.7$) monotonously decreases from $2.65\mu_B/\text{f.u.}$ for 10% Ga substitution to $0.64\mu_B/\text{f.u.}$ for 70% Ga content (Fig. 10, open squares). The assumption of a perfectly ordered sublattice of Fe^{3+} , Ga^{3+} , and Re^{5+} cations with ferromagnetic interactions within each of the two sublattices—Fe/Ga and Re—and antiferromagnetic interactions between the two sublattices leads to the following expectation for the saturation magnetization behavior: a continuous decrease from $2.5\mu_B/\text{f.u.}$ for 10% Ga substitution to $0\mu_B/\text{f.u.}$ for 60% Ga content, with a subsequent increase to $0.5\mu_B/\text{f.u.}$ for 70% Ga substitution (Fig. 10, solid circles). Apparently, the observed trend disagrees with (i) the experimentally observed dependence of the saturation magnetization from the Ga content of the sample and (ii) the results of the Rietveld refinement which indicate an increasing amount of disorder with increasing Ga content in both phases—the tetragonal and the cubic one.

The simulated saturation magnetization of $\text{Sr}_2\text{Fe}_{1-x}\text{Ga}_x\text{ReO}_6$ (Fig. 10, solid squares) is estimated as a function of the Ga/Re and Fe/Re antisite disorder based on

the following experimental results and assumptions: (i) the saturation magnetization is calculated for the tetragonal and cubic phases separately, (ii) the total saturation magnetization of samples comprised of a tetragonal and a cubic phase is calculated by taking into account the relative fraction of tetragonal and cubic phases in the sample, (iii) the amount of antisite disorder of each sample was taken from the results of the Rietveld refinement (Table I), and (iv) a ferromagnetic interaction is assumed within both sublattices and an antiferromagnetic interaction between them. The saturation magnetization obtained in this way decreases from $2.66\mu_B/\text{f.u.}$ to $0.24\mu_B/\text{f.u.}$ in the concentration range between 10% and 70% Ga (Fig. 10, solid squares).

The observed behavior leads to the conclusion that the concentration dependence of the saturation magnetization for $\text{Sr}_2\text{Fe}_{1-x}\text{Ga}_x\text{ReO}_6$ ($0 < x < 0.7$) can be modeled correctly by considering the crystal structure as obtained by Rietveld refinement. Thus, a combination of x-ray refinements and magnetic susceptibility measurements confirms the presence of a concentration-dependent antisite disorder. This result is unexpected because it is in contradiction to earlier results from investigations on solid solutions of

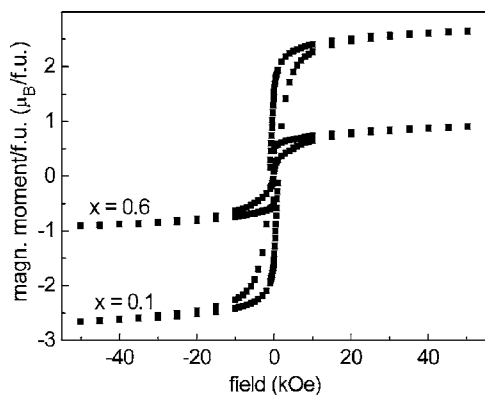


FIG. 9. Magnetic hysteresis loops of $\text{Sr}_2\text{Fe}_{1-x}\text{Ga}_x\text{ReO}_6$ measured at 5 K.

$\text{Sr}_2\text{Fe}_{1-x}\text{M}'_x\text{Re}_{1-y}\text{M}''_y\text{O}_6$ reported earlier, which do not show any antisite disorder.^{30,40–42}

From the magnetic susceptibility measurements, performed between 780 K and 5 K at 0.1 T, Curie temperatures T_C were determined to be in the range between 365 K and 401 K. In contrast to the saturation magnetization the T_C values indicate no systematic trend as a function of the Ga content. In order to verify this finding, additional batches of samples were prepared. Magnetic measurements of these samples confirmed the strong dependence of the correlation between T_C and the Ga content upon the sample preparation history. The distribution of the cubic and tetragonal phases is dependent upon the relative velocities of the quenching procedure and the site exchange. Because a macroscopic sample always exhibits a temperature gradient, it is difficult to prepare a homogeneous sample.

Ga-substituted samples reveal ferrimagnetic behavior in the total concentration range examined in this study, because the paramagnetic regime of the high-temperature magnetic susceptibility data could only be interpreted using a ferrimagnetic model. The results of the fits were used to extract the ferrimagnetic (T_C) and paramagnetic (Θ_C) Curie temperatures and interaction parameter (μ) as well as Curie con-

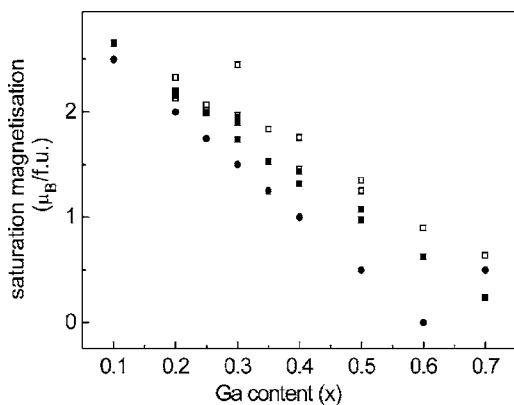


FIG. 10. Experimental saturation magnetization (\square) of $\text{Sr}_2\text{Fe}_{1-x}\text{Ga}_x\text{ReO}_6$ ($0 < x < 0.7$) together with the simulated saturation magnetization of (\bullet) the ordered $\text{Sr}_2\text{Fe}_{1-x}\text{Ga}_x\text{ReO}_6$, and (\blacksquare) $\text{Sr}_2\text{Fe}_{1-x}\text{Ga}_x\text{ReO}_6$ with the disorder value as obtained by Rietveld refinement as a function of the Ga content.

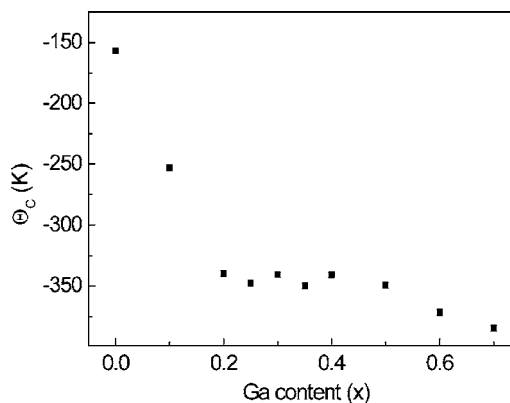


FIG. 11. Paramagnetic Curie temperature Θ_C versus Ga content.

stants (C_A, C_B) for the two sublattices A and B for $\text{Sr}_2\text{Fe}_{1-x}\text{Ga}_x\text{ReO}_6$ ($0.1 < x < 0.7$). The standard function describing the molar susceptibility χ_M in molecular field approximation has been applied:⁴³

$$\chi_M = \frac{(C_A + C_B)T - 2\mu C_A C_B}{T^2 - T_C^2},$$

with

$$\Theta_C = -\frac{2\mu C_A C_B}{C_A + C_B}$$

and

$$T_C^2 = \mu^2 C_A C_B.$$

The paramagnetic Curie temperature Θ_C changes from -157 K for the parent compound to -340 K for the sample containing 20% Ga. Between 20% and 40% Ga content, Θ_C shows a weak concentration dependence, whereas it decreases slightly for $0.4 < x < 0.7$ (Fig. 11). The weak temperature dependence for $0.2 < x < 0.4$ can be explained by assuming itinerant magnetism whereas the slight decrease of Θ_C for $0.4 < x < 0.7$ can be related to the appearance of the cubic second phase.^{22,23}

The Curie constants C_A and C_B for the two sublattices A and B reveal an opposite dependence on the Ga content (Fig. 12). Whereas C_A decreases from $8.7 \text{ cm}^3 \text{ K mol}^{-1}$ to $5.3 \text{ cm}^3 \text{ K mol}^{-1}$, C_B increases from $1.2 \text{ cm}^3 \text{ K mol}^{-1}$ to $3.4 \text{ cm}^3 \text{ K mol}^{-1}$ with increasing Ga content; i.e., the values for C_A and C_B show a tendency to converge. This behavior is in line with the change of the chemical compositions of the two sublattices. Together with the decrease of the Fe content for these compounds, the Re/Ga disorder increases with increasing doping level. In other words, the chemical compositions of the two sublattices—Fe/Ga and Re—become more similar upon Ga substitution. Moreover, the absolute values of C_A and C_B for $\text{Sr}_2\text{Fe}_{0.9}\text{Ga}_{0.1}\text{ReO}_6$ are in good agreement with the values obtained for $\text{Sr}_2\text{FeRe}_{0.9}\text{Sb}_{0.1}\text{O}_6$.²³

D. Mössbauer measurements

^{57}Fe -Mössbauer spectra of the samples with $x < 0.35$ exhibit magnetic sextet patterns with relatively narrow lines

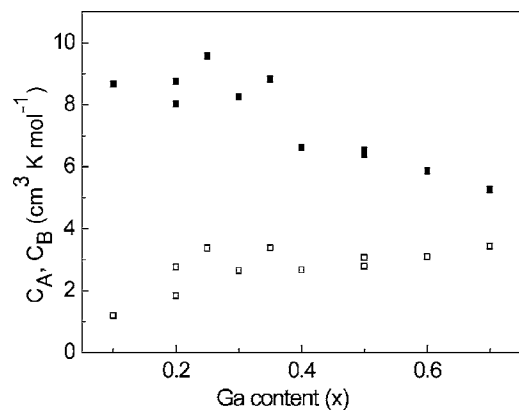


FIG. 12. Curie constants C_A (■) and C_B (□) of the two sublattices A and B versus Ga content.

corresponding to the only Fe site in symmetrical environment. In the concentration range $0.35 < x < 0.7$, a paramagnetic component with relative intensity of about 10% appears in addition to the magnetic sextet (Fig. 13). The isomer shift value of the sextet $\delta = 0.66(1) \text{ mm s}^{-1}$ remains constant over the total range of concentrations. The hyperfine magnetic field of $465(2) \text{ kOe}$ is constant up to a Ga content of 35% and decreases slowly at higher Ga concentrations, attaining the value $461(1) \text{ kOe}$ at $x = 0.7$. Taking into account the results of the magnetic measurements, one can conclude that in spite of the paramagnetic component all spectra correspond to magnetically ordered phases. Sharp Mössbauer lines exclude a considerable amount of microscopic disorder involving Fe atoms.

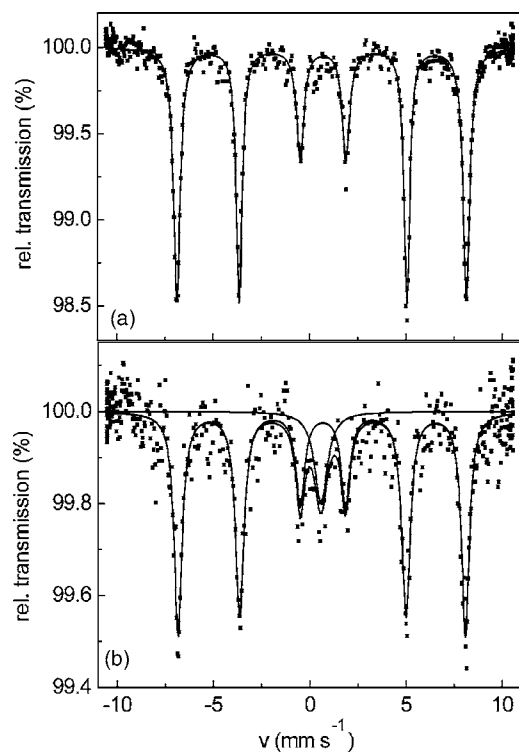


FIG. 13. ^{57}Fe Mössbauer spectra of $\text{Sr}_2\text{Fe}_{1-x}\text{Ga}_x\text{ReO}_6$: (a) $x = 0.2$, (b) $x = 0.5$.

The average valence state of Fe can be estimated by comparing the isomer shift of the series $\text{Sr}_2\text{Fe}_{1-x}\text{Ga}_x\text{ReO}_6$ with the isomer shift of the parent compound, $\delta(\text{Fe}, x=0) = 0.67(1) \text{ mm s}^{-1}$.^{22,23} Thus, the Fe valence state remains constant at 2.7+ for the whole series leaving the role of the electronic buffer element to Re.

IV. DISCUSSION

In order to put our results into context we recollect the most important findings from x-ray diffraction and magnetic susceptibility measurements. (i) There is a phase separation of one metastable tetragonal phase into one tetragonal and one cubic phase for Ga content $x \geq 0.4$. The phase distribution is determined by the cooling rate during the preparation of the primary metastable tetragonal phase rather than by the Ga content. (ii) The paramagnetic Curie temperature Θ_C depends upon the Ga concentration as shown in Fig. 11. (iii) For Ga content $x \geq 0.4$ a paramagnetic phase develops in addition to the magnetically ordered tetragonal phase.

Therefore, we propose that, depending on the Ga content, two different phases exist. For small Ga concentrations ($x \leq 0.2$), Ga substitutes Fe in a statistical fashion and disturbs the magnetic double exchange between Fe-based and Re-based magnetic sublattices. The value $x = 0.2$ directly follows from the concentrational dependence of Θ_C (Fig. 11) and indicates the incipient phase separation. For $0.2 \leq x \leq 0.4$, $\text{Sr}_2\text{Fe}_{1-x}\text{Ga}_x\text{ReO}_6$ separates into two phases. This separation is not yet detectable by x-ray diffraction or Mössbauer spectroscopy but only by the independence of Θ_C from the Ga content. For $x \geq 0.4$, the Mössbauer spectra indicate the appearance of a second paramagnetic phase. This threshold is in accordance with the appearance of a second highly disordered, cubic phase detected by x-ray diffraction. This phase appears to be paramagnetic because the large amount of antisite disorder enables the Fe atoms to be surrounded by diamagnetic Ga atoms. As a consequence, these Fe atoms reveal no hyperfine magnetic field. Presumably, the process of phase separation for $x < 0.4$ cannot be traced by means of Mössbauer spectroscopy and x-ray diffraction due to the absence of Fe atoms in the paramagnetic, probably Ga-based phase and the small amount of this phase in the sample, respectively. The increasing amount of antisite disorder also explains the fact that we do not observe Fe species with intermediate values of the hyperfine magnetic field originating from configurations with different numbers of diamagnetic Ga neighbors in the first coordination sphere of the Fe atoms.

The interesting fact that the hyperfine field is constant and independent of the extent of diamagnetic Ga dilution has attracted special attention. As mentioned above, Re adopts the role of an electronic buffer and provides the stability of the Fe valence state over a wide range of Ga substitutions. The hyperfine magnetic field on the Fe nuclei mainly depends on the Fermi contact term which depends on the imbalance of the s electrons. Therefore, the constant density of s electrons detected in the Mössbauer experiments is the reason for the concentrational independence of the hyperfine magnetic field. It seems that the magnetic order is an impor-

tant precondition, which leads to a constant hyperfine magnetic field even in Ga-rich samples.

V. CONCLUSION

In this study we explored the effect of diamagnetic dilution of the Fe sublattice on the structural and magnetic properties of the double perovskite $\text{Sr}_2\text{Fe}_{1-x}\text{Ga}_x\text{ReO}_6$ ($0 < x < 0.7$) by means of x-ray structural analysis, magnetometry, Mössbauer spectroscopy, and band structure calculations. An unexpected finding is the observation that Ga not only occupies the Fe but also the Re lattice site. As a result, a Ga/Re antisite disorder is observed, which is dependent on the Ga content. It is a well-established fact that the parent compound $\text{Sr}_2\text{FeReO}_6$ exhibits virtually no Fe/Re (M/M') disorder. On the other hand, Fe^{3+} can easily be substituted by Ga^{3+} because of the similarity of the ionic radii, and it is for this reason that Ga^{3+} is used for the diamagnetic dilution of ferric oxides or sulfides. Although the amount of antisite disorder increases with increasing Ga content, it is also strongly determined by the cooling velocity during the sample preparation. For $0 < x < 0.4$ only one tetragonal, magnetically ordered phase was detected by x-ray structural analysis, in agreement with Mössbauer spectroscopic data. For $x \geq 0.4$, a phase separation into one tetragonal and one cubic phase is detected by x-ray structural analysis. These findings are confirmed by the presence of a magnetically ordered and a paramagnetic phase in the corresponding Mössbauer spectra. In

summary, the experimental data suggest the formation of two phases: a ferrimagnetic tetragonal one and paramagnetic cubic one. Below 20% Ga content, Ga statistically enters the -Fe-O-Re-O-Fe- double-exchange pathways. Phase separation appears above 20% Ga substitution; between 20% and 40% Ga content, the paramagnetic Ga-based phase appears not to contain any Fe. The Fe-containing cubic and paramagnetic phases detected by Mössbauer spectroscopy first appear for the composition $\text{Sr}_2\text{Fe}_{0.6}\text{Ga}_{0.4}\text{ReO}_6$.

Due to the Ga-content-dependent Ga/Re disorder, a phase with itinerant magnetic behavior (as in the parent compound $\text{Sr}_2\text{FeReO}_6$) coexists with a paramagnetic phase. Re adopts the role of an electronic buffer element, which keeps the valence state of Fe constant over a wide Ga substitution range. Therefore, Re should be viewed as the basic magnetic element which provides the static ferrimagnetic order for higher Ga substitution levels. The end member of the substitution series $\text{Sr}_2\text{Fe}_{1-x}\text{Ga}_x\text{ReO}_6$, $\text{Sr}_2\text{GaReO}_6$, is predicted to be a half-metallic ferromagnet although it contains no magnetic elements. All attempts to synthesize this compound as a pure single-phase solid have failed so far.

ACKNOWLEDGMENTS

This work was supported by the Deutsche Forschungsgemeinschaft (Forschergruppe 559) and the Materials Science Center (MWFZ) at the Johannes-Gutenberg Universität Mainz.

-
- ¹K.-I. Kobayashi, T. Kimura, H. Sawada, K. Terakura, and Y. Tokura, *Nature (London)* **395**, 677 (1998).
²K.-I. Kobayashi, T. Kimura, Y. Tomioka, H. Sawada, K. Terakura, and Y. Tokura, *Phys. Rev. B* **59**, 11159 (1999).
³J. Cibert, J.-F. Bobo, and U. Lüders, *C. R. Phys.* **6**, 977 (2005).
⁴J. J. Attema, L. Chioncel, C. M. Fang, G. A. de Wijs, and R. A. de Groot, *Lect. Notes Phys.* **678**, 201 (2005).
⁵J. Longo and R. Ward, *J. Am. Chem. Soc.* **83**, 2816 (1961).
⁶W. Kockelmann, D. T. Adroja, A. D. Hillier, M. Wakeshima, Y. Izumiyama, Y. Hinatsu, K. S. Knight, D. Visser, and B. D. Rainford, *Physica B* **378–380**, 543 (2006).
⁷N. Rammeh, K. G. Bramnik, H. Ehrenber, C. Ritter, H. Fuess, and A. Cheikh-Rouhou, *Phys. Status Solidi C* **1**, 1669 (2004); N. Rammeh, H. Ehrenberg, H. Fuess, and A. Cheikh-Rouhou, *Phys. Status Solidi C* **3**, 3225 (2006).
⁸Q. Lin, M. Greenblatt, and M. Croft, *J. Solid State Chem.* **178**, 1356 (2005).
⁹K. Kuepper, I. Balasz, H. Hesse, A. Winiarski, K. C. Prince, M. Matteucci, D. Wett, R. Szargan, E. Burzo, and M. Neumann, *Phys. Status Solidi A* **201**, 3252 (2004).
¹⁰M. C. Viola, M. J. Martinez-Lope, J. A. Alonso, J. L. Martinez, J. M. De Paoli, S. Pagola, J. C. Pedregosa, M. T. Fernandez-Diaz, and R. E. Carbonio, *Chem. Mater.* **15**, 1655 (2003).
¹¹T. Hernandez, F. Plazaola, J. M. Barandiaran, and J. M. Greneche, *Hyperfine Interact.* **161**, 113 (2005).
¹²G. Popov, M. V. Lobanov, V. Maxim, and E. V. Tsiper, *J. Phys.: Condens. Matter* **16**, 135 (2004).
¹³D. D. Sarma, E. V. Sampathkumaran, S. Ray, R. Nagarajan, S. Majumdar, A. Kumar, G. Nalini, and T. N. G. Row, *Solid State Commun.* **114**, 465 (2000).
¹⁴C. Ritter, M. R. Ibarra, L. Morellon, J. Blasco, J. Garcia, and J. M. De Teresa, *J. Phys.: Condens. Matter* **12**, 8295 (2000); E. Carvajal, O. Navarro, R. Allub, M. Avignon, and B. Alascio, *Phys. Status Solidi B* **242**, 1942 (2005).
¹⁵Z. Fang, K. Terakura, and J. Kanamori, *Phys. Rev. B* **63**, 180407(R) (2001).
¹⁶C. Zener, *Phys. Rev.* **81**, 440 (1951); **82**, 403 (1951); **83**, 299 (1951); **85**, 324 (1952).
¹⁷F. Sher, A. Venimadhav, M. G. Blamire, B. Dabrowski, S. Kolesnik, and J. P. Attfield, *Solid State Sci.* **7**, 912 (2005).
¹⁸J. B. Goodenough, *Magnetism and the Chemical Bond* (Interscience, New York, 1966).
¹⁹S. Wurmehl, H. C. Kandpal, G. H. Fecher, and C. Felser, *J. Phys.: Condens. Matter* **18**, 6171 (2006).
²⁰K. G. Bramnik, H. Ehrenberg, J. K. Dehn, and H. Fuess, *Solid State Sci.* **5**, 235 (2003).
²¹H. Kato, T. Okuda, Y. Okimoto, Y. Tomioka, K. Oikawa, T. Kamiyama, and Y. Tokura, *Phys. Rev. B* **69**, 184412 (2004).
²²A. Jung, I. Bonn, V. Ksenofontov, G. Melnyk, J. Ensling, C. Felser, and W. Tremel, *J. Mater. Chem.* **15**, 1760 (2005).
²³A. Jung, V. Ksenofontov, S. Reiman, H. A. Therese, U. Kolb, C. Felser, and W. Tremel, *Phys. Rev. B* **73**, 144414 (2006).
²⁴J. Cheng and Z. Q. Yang, *Phys. Status Solidi B* **243**, 1151 (2006).
²⁵P. Majewski, S. Geprags, A. Boger, M. Opel, A. Erb, R. Gross, G.

- Vaitheeswaran, V. Kanchana, A. Delin, F. Wilhelm, A. Rogalev, and L. Alff, *Phys. Rev. B* **72**, 132402 (2005).
- ²⁶Y. Tomioka, T. Okuda, Y. Okimoto, R. Kumai, K.-I. Kobayashi, and Y. Tokura, *Phys. Rev. B* **61**, 422 (2000).
- ²⁷T. H. Kim, M. Uehara, S.-W. Cheong, and S. Lee, *Appl. Phys. Lett.* **74**, 1737 (1999).
- ²⁸A. W. Sleight and J. F. Weiher, *J. Phys. Chem. Solids* **33**, 679 (1972).
- ²⁹A. W. Sleight, J. Longo, and R. Ward, *Inorg. Chem.* **1**, 245 (1962).
- ³⁰H. Kato, T. Okuda, Y. Okimoto, Y. Tomioka, K. Oikawa, T. Kamiyama, and Y. Tokura, *Phys. Rev. B* **65**, 144404 (2002).
- ³¹P. Blaha, K. Schwarz, G. K. H. Madsen, D. Kvasnicka, and J. Luitz, WIEN2k, An augmented plane wave+local orbitals program for calculating crystal properties, Karlheinz Schwarz, Technical Universität Wien, Austria, 2001.
- ³²R. W. Cheary and A. Coelho, *J. Appl. Crystallogr.* **25**, 109 (1992); A. Coelho, computer code TOPAS, Academic 1.0, 2004.
- ³³W. Haberditzl, *Magnetochemie* (Akademie-Verlag, Berlin, 1968).
- ³⁴K. Lagarec and D. G. Rancourt, *Nucl. Instrum. Methods Phys. Res. B* **129**, 266 (1997).
- ³⁵T. J. Gray, *J. Power Sources* **6**, 121 (1981).
- ³⁶R. Scholder and P. P. Pfeiffer, *Angew. Chem., Int. Ed. Engl.* **2**, 265 (1963).
- ³⁷R. D. Shannon, *Acta Crystallogr., Sect. A: Cryst. Phys., Diffr., Theor. Gen. Crystallogr.* **32**, 751 (1976).
- ³⁸G. Popov, M. Greenblatt, and M. Croft, *Phys. Rev. B* **67**, 024406 (2003).
- ³⁹U. Müller, *Anorganische Strukturchemie* (Teubner Studienbücher, Stuttgart, 1996).
- ⁴⁰W. Prellier, V. Smolyaninova, A. Biswas, C. Galley, R. L. Greene, K. Ramesha, and J. Gopalakrishnan, *J. Phys.: Condens. Matter* **12**, 965 (2000); A. Poddar and S. Das, *Physica B* **344**, 325 (2004).
- ⁴¹J. Gopalakrishnan, A. Chattopadhyay, S. B. Ogale, T. Venkatesan, R. L. Greene, A. J. Millis, K. Ramesha, B. Hannoyer, and G. Marest, *Phys. Rev. B* **62**, 9538 (2000).
- ⁴²N. Rammeh, K. G. Bramnik, H. Ehrenberg, H. Fuess, and A. Cheikh-Rouhou, *J. Magn. Magn. Mater.* **278**, 14 (2004).
- ⁴³C. Kittel, *Introduction to Solid State Physics* (VCH Wiley, New York, 1976).